JOM 23479

# Bidentate ligand substitution in $PhCCo_3(CO)_9$. Synthesis, molecular structure, and redox reactivity of $PhCCo_3(CO)_7$(*cis*-$Ph_2PCH{=}CHPPh_2$)

Kaiyuan Yang, Simon G. Bott and Michael G. Richmond

*Center for Organometallic Research and Education, Department of Chemistry, University of North Texas, Denton, TX 76203 (USA)*

(Received September 25, 1992; in revised form November 30, 1992)

**Abstract**

The synthesis of $PhCCo_3(CO)_7$(*cis*-$Ph_2PCH{=}CHPPh_2$) (**2**) from $PhCCo_3(CO)_9$ (**1**) and the bidentate phosphine *cis*-$Ph_2PCH{=}CHPPh_2$ is described. Cluster **2** is readily prepared in moderate to high yield using a variety of procedures. The diphosphine ligand in **2** bridges adjacent cobalt atoms as shown by $^{13}C$ and $^{31}P$ NMR spectroscopic measurements and X-ray diffraction analysis. $PhCCo_3(CO)_7$(*cis*-$Ph_2PCH{=}CHPPh_2$) crystallizes in the monoclinic space group $P2_1/c$ with $a = 12.7065$ (9), $b = 18.385$ (2), $c = 15.943$ (1) Å, $\beta = 98.025$ (6)°, $V = 3688.0$ (5) Å$^3$, and $Z = 4$. Full-matrix least-squares refinement yielded $R = 0.0445$ for 2021 ($I > 3\sigma(I)$) reflections. The redox properties of **2** have been examined by using cyclic and rotating disk electrode voltammetric techniques. In $CH_2Cl_2$ solvent, **2** exhibits reversible $0/-1$ and $0/+1$ redox couples. The reversibility of the $0/+1$ redox couple is highly dependent on the temperature and the nature of the solvent. Use of MeCN or THF as solvent leads to an irreversible, multi-electron oxidation. The electrochemistry of **2** is compared to the known cluster $PhCCo_3(CO)_7$(dppe).

## 1. Introduction

Bidentate-phosphine ligand substitution in alkylidyne-bridged tricobalt clusters, $RCCo_3(CO)_9$, continues to be investigated in connection with hydroformylation catalysis [1,2] and redox reactivity [3–5] and NMR fluxionality studies [6]. In these cases, the diphosphine ligand serves to bridge adjacent cobalt atoms via equatorial coordination. However, this mode of substitution is dependent on the nature of the ancillary phosphine. For example, the reaction between $PhCCo_3(CO)_9$ and 1,1′-bis(diphenylphosphino)ferrocene (dppf) affords the axially bridged cluster $PhCCo_3(CO)_7$(dppf), the molecular structure of which has been determined by X-ray diffraction analysis [7]. The coordination mode adopted by the dppf ligand is driven by minimization of unfavorable intramolecular contacts between the dppf and $\mu_3$-benzylidyne capping ligands.

Recently, we have examined the reaction between $PhCCo_3(CO)_9$ (**1**) and 2,3-bis(diphenylphosphino) maleic anhydride (bma) in the hope of preparing the diphosphine-substituted cluster $PhCCo_3(CO)_7$(bma), a cluster that should exhibit novel redox properties due to the presence of the ancillary bma ligand [8–14]. However, the anticipated cluster $PhCCo_3(CO)_7$(bma) was not observed, but rather the new cluster $Co_3(CO)_6\{\mu_2\text{-}\eta^2\text{-}\eta^1\text{-}\overline{C(Ph)C{=}C(PPh_2)C(O)OC(O)}\}(\mu_2\text{-}PPh_2)$, which possesses a six-electron $\mu_2$-benzylidene-$\eta^2$-$\eta^1$-(diphenylphosphino)maleic anhydride ligand, was isolated [15]. The reason for this unusual ligand transformation is not currently known but it most likely stems from an electronic effect associated with the bma ligand. Accordingly, we sought to prepare a suitable cluster derivative that would enable us to test this hypothesis. The unsaturated diphosphine cluster $PhCCo_3(CO)_7$(*cis*-$Ph_2PCH{=}CHPPh_2$), which is expected to be structurally similar yet electronically different compared to the unobserved cluster $PhCCo_3(CO)_7$(bma), represents one such model cluster compound.

In this paper we describe the synthesis and spectral and X-ray crystallographic characterization of the ligand-bridged cluster $PhCCo_3(CO)_7$(*cis*-$Ph_2PCH{=}CHPPh_2$) (**2**). The redox properties of **2** have been examined by cyclic and rotating disk electrode techniques, which indicate that **2**, with its unsaturated diphosphine ligand, behaves similarly to the known

Correspondence to: Dr. S.G. Bott or Dr. M.G. Richmond.

0022-328X/93/$6.00

saturated diphosphine cluster $PhCCo_3(CO)_7$(dppe)[3]. The effect of polar solvents on the 0/+1 redox state in **2** is discussed.

## 2. Results and discussion

### 2.1. Synthesis and spectroscopic data for $PhCCo_3(CO)_7$(*cis*-$Ph_2PCH$=$CHPPh_2$)

A clean reaction between $PhCCo_3(CO)_9$ [16] and *cis*-$Ph_2PCH$=$CHPPh_2$ was observed when equimolar amounts of reactants were heated overnight at 75°C (eqn. (1)). TLC analysis revealed the presence of a slower moving material that is readily assigned to the product cluster, $PhCCo_3(CO)_7$(*cis*-$Ph_2PCH$=$CHPPh_2$). Cluster **2** was subsequently isolated in 75% yield by chromatography using silica gel and $CH_2Cl_2$/petroleum ether. Alternative synthetic methods were also examined as a route to cluster **2**. $Me_3NO$-promoted oxidative decarbonylations [17] and sodiobenzophenone ketyl-initiated electron-transfer chain (ETC) reactions [18] also gave cluster **2** in isolated yields that ranged from 50 to 70%.

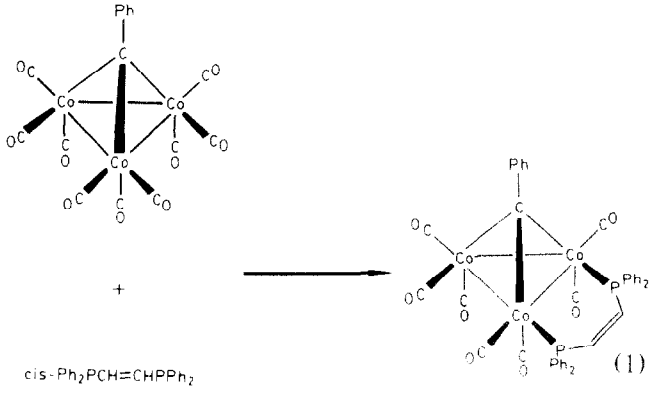


The IR spectrum of **2** in $CH_2Cl_2$ revealed two prominent $\nu$(CO) bands at 2057s and 2006vs $cm^{-1}$, which are assigned to terminal carbonyl groups, along with a very weak $\nu$(CO) band at 1831 $cm^{-1}$. The intensity pattern and frequency of these terminal carbonyl bands are in agreement with the IR data reported for the diphosphine-bridged cluster $PhCCo_3(CO)_7$(dppe) [3]. The $^{31}P\{^1H\}$ NMR spectrum of an *in situ* generated sample of **2**, recorded at 233 K, exhibited a major (> 95%) $^{31}P$ resonance at $\delta$36.2 along with a pair of equal intensity resonances at $\delta$ 77.7 and 103.6. The major resonance is assigned to cluster **2** with a bridging diphosphine ligand while the minor species is ascribed to the isomeric cluster which is substituted with a chelating diphosphine ligand. A chelating diphosphine ligand in **2** may be rationalized

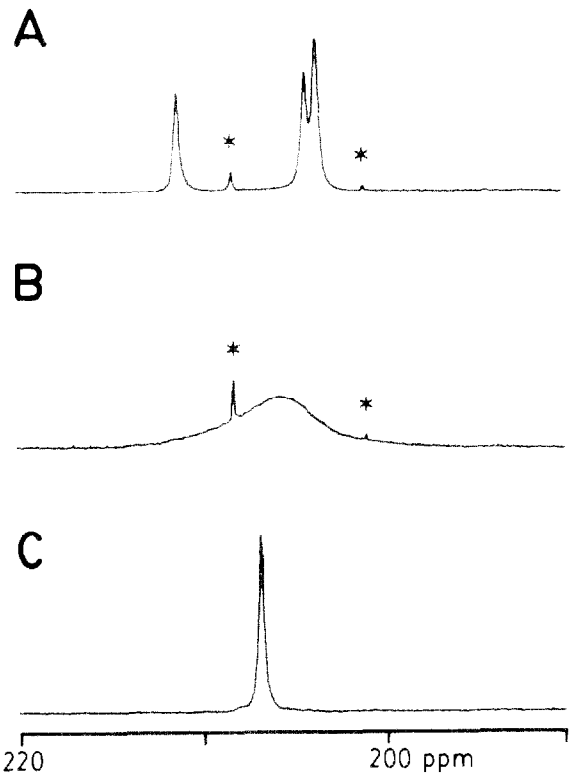


Fig. 1. Variable-temperature $^{13}C\{^1H\}$ NMR spectra of the carbonyl region of $PhCCo_3(CO)_7$(*cis*-$Ph_2PCH$=$CHPPh_2$) in THF/benzene-$d_6$ (5:1) at (A) 185 K, (B) 216 K, and (C) 298 K. The marked resonances represent the carbonyl groups associated with the chelated diphosphine cluster **2**.

due to the existence of two highly deshielded, inequivalent $^{31}P$ resonances [19,20].

The variable-temperature $^{13}C\{^1H\}$ NMR behavior of **2** was examined next by using a sample of **2** that was ~ 20–30% enriched in $^{13}CO$. Figure 1 shows the $^{13}C$ NMR spectra of **2**. The limiting spectrum of **2** in Fig. 1(A) reveals the presence of three terminal carbonyl resonances at $\delta$ 211, 204, and 203 with a relative integral ratio of 2:2:3, respectively. The two resonances at $\delta$ 211 and 204 are assigned to the pairwise equivalent axial and equatorial carbonyl groups at the phosphine-substituted cobalt centers [6,21]. The remaining high-field resonance at $\delta$ 203 represents the carbonyls associated with the cobalt tricarbonyl group, which are rendered magnetically equivalent as a result of rapid, intramolecular 3-fold carbonyl scrambling [22]. As the temperature is raised to 216 K, the carbonyl resonances broaden, more or less at the same rate, and merge to give a single, broad resonance at $\delta$ 206, which is in agreement with the weighted-average chemical shift. Further warming to room temperature promotes rapid, intramolecular carbonyl scrambling about the cluster polyhedron; this gives rise to the $^{13}C$ NMR

TABLE 1. X-ray crystallographic and data processing parameters for $PhCCo_3(CO)_7$(*cis*-$Ph_2PCH{=}CHPPh_2$) (**2**)

| | |
|---|---|
| Space group | $P2_1/c$ (monoclinic) |
| Cell constants | |
| $a$(Å) | 12.7065(9) |
| $b$(Å) | 18.385(2) |
| $c$(Å) | 15.943(1) |
| $\beta$(°) | 98.025(6) |
| $V$(Å$^3$) | 3688.0(5) |
| Molecular formula | $C_{40}H_{27}Co_3O_7P_2$ |
| F.W. | 858.40 |
| Formula units/cell ($Z$) | 4 |
| $\rho$ (g cm$^{-3}$) | 1.546 |
| Crystal size (mm$^3$) | 0.08×0.22×0.43 |
| Absorption coefficient ($\mu$) (cm$^{-1}$) | 14.65 |
| $\lambda$ (radiation) (Å) | 0.71073 |
| Data collection method | $\theta$–$2\theta$ |
| Collection range (°) | $2.0 \leq 2\theta \leq 44.0$ |
| Total no. of data collected | 4786 |
| No. of independent data, $I > 3\sigma(I)$ | 2021 |
| $R$ | 0.0445 |
| $R_w$ | 0.0488 |
| Weights | $w = [(\sigma F_o)^2]^{-1}$ |

spectrum shown in Fig. 1(C) [23*]. Using the CO exchange pathways proposed by McGlinchey [6] for related tetrahedrane clusters along with the knowledge of the limiting $^{13}C$ chemical shifts and the coalescence temperature, $\tau_c$, we estimate that complete carbonyl scrambling in **2** occurs with an activation energy of ~9.6 kcal/mol [24]. This value for $\Delta G^{\ddagger}$ in **2** is in excellent agreement with the data reported by McGlinchey [6].

### 2.2. *X-ray crystallographic structure of* $PhCCo_3(CO)_7$ (*cis*-$Ph_2PCH{=}CHPPh_2$)

The bonding mode of the diphosphine ligand in **2** was established by single-crystal X-ray diffraction analysis. Black crystals of **2** were grown from a $CH_2Cl_2$ solution containing **2** that had been layered with heptane. Compound **2** exists as discrete molecules in the unit cell with no unusually short inter- or intramolecular contacts. The X-ray data collection and processing parameters for **2** are given in Table 1 with the final fractional coordinates listed in Table 2.

The ORTEP diagram in Fig. 2 shows the molecular structure of **2** and establishes the equatorial disposition of the bridging *cis*-$Ph_2PCH{=}CHPPh_2$ ligand. No bridging carbonyls are observed in agreement with the IR

* Reference number with asterisk indicates a note in the list of references.

TABLE 2. Positional parameters of the non-hydrogen atoms for $PhCCo_3(CO)_7$(*cis*-$Ph_2PCH{=}CHPPh_2$) (**2**) with estimated standard deviations in parentheses

| Atom | $x$ | $y$ | $z$ | $U$ [a] |
|---|---|---|---|---|
| Co1 | 0.8269(1) | 0.05193(8) | 0.33533(9) | 2.94(3) |
| Co2 | 0.6485(1) | −0.00429(8) | 0.32084(9) | 3.01(3) |
| Co3 | 0.7051(1) | 0.08093(9) | 0.43964(9) | 3.63(4) |
| P1 | 0.8672(2) | 0.0500(2) | 0.2052(2) | 2.85(6) |
| P2 | 0.6151(2) | −0.0295(2) | 0.1844(2) | 2.90(6) |
| O1 | 0.9779(7) | 0.1660(5) | 0.3945(6) | 6.4(2) |
| O2 | 0.9383(7) | −0.0700(5) | 0.4274(6) | 6.7(2) |
| O3 | 0.7056(7) | −0.1449(4) | 0.4017(5) | 5.7(2) |
| O4 | 0.4258(6) | −0.0059(6) | 0.3437(5) | 6.7(2) |
| O5 | 0.4954(8) | 0.1069(6) | 0.4872(6) | 7.3(3) |
| O6 | 0.8024(9) | −0.0164(7) | 0.5755(6) | 9.8(3) |
| O7 | 0.774(1) | 0.2288(6) | 0.4829(7) | 10.6(4) |
| C1 | 0.9175(9) | 0.1212(7) | 0.3692(7) | 4.3(3) |
| C2 | 0.8950(9) | −0.0244(6) | 0.3881(7) | 4.0(3) |
| C3 | 0.6853(9) | −0.0906(6) | 0.3685(7) | 3.7(3) |
| C4 | 0.5142(9) | −0.0039(7) | 0.3338(7) | 4.2(3) |
| C5 | 0.578(1) | 0.0957(7) | 0.4669(8) | 4.6(3) |
| C6 | 0.763(1) | 0.0212(9) | 0.5228(8) | 6.2(4) |
| C7 | 0.749(1) | 0.1687(8) | 0.4673(8) | 6.2(4) |
| C8 | 0.7601(8) | 0.0628(5) | 0.1184(6) | 2.6(2) |
| C9 | 0.6662(8) | 0.0317(6) | 0.1109(6) | 2.9(2) |
| C10 | 0.6913(8) | 0.0946(5) | 0.3179(6) | 2.6(2) |
| C11 | 0.6411(8) | 0.1589(5) | 0.2714(6) | 2.9(2) |
| C12 | 0.5315(9) | 0.1704(6) | 0.2592(7) | 4.0(3) |
| C13 | 0.488(1) | 0.2295(7) | 0.2132(9) | 5.4(4) |
| C14 | 0.551(1) | 0.2792(6) | 0.1805(9) | 5.2(3) |
| C15 | 0.659(1) | 0.2709(6) | 0.1936(8) | 5.2(3) |
| C16 | 0.704(1) | 0.2114(7) | 0.2406(8) | 4.5(3) |
| C111 | 0.9616(9) | 0.1205(6) | 0.1818(7) | 3.6(2) * |
| C112 | 0.9317(9) | 0.1827(7) | 0.1380(7) | 4.3(3) * |
| C113 | 1.009(1) | 0.2338(8) | 0.1219(9) | 6.0(3) * |
| C114 | 1.111(1) | 0.2200(8) | 0.1491(9) | 6.0(3) * |
| C115 | 1.145(1) | 0.1608(8) | 0.1935(9) | 6.1(3) * |
| C116 | 1.069(1) | 0.1089(7) | 0.2109(8) | 4.9(3) * |
| C117 | 0.9315(8) | −0.0307(6) | 0.1673(7) | 3.4(2) * |
| C118 | 0.9204(9) | −0.0465(7) | 0.0823(7) | 4.3(3) * |
| C119 | 0.969(1) | −0.1056(7) | 0.0520(8) | 5.1(3) * |
| C120 | 1.028(1) | −0.1500(7) | 0.1066(8) | 5.2(3) * |
| C121 | 1.045(1) | −0.1366(8) | 0.1899(8) | 5.8(3) * |
| C122 | 0.995(1) | −0.0759(7) | 0.2227(7) | 4.7(3) * |
| C211 | 0.4739(8) | −0.0275(6) | 0.1482(7) | 3.4(2) * |
| C212 | 0.415(1) | −0.0884(7) | 0.1562(8) | 4.9(3) * |
| C213 | 0.302(1) | −0.0844(8) | 0.1386(8) | 5.6(3) * |
| C214 | 0.256(1) | −0.0218(7) | 0.1143(8) | 5.3(3) * |
| C215 | 0.313(1) | 0.0391(7) | 0.1034(8) | 4.9(3) * |
| C216 | 0.4233(9) | 0.0355(6) | 0.1209(7) | 3.6(2) * |
| C217 | 0.6570(9) | −0.1165(6) | 0.1439(6) | 3.4(2) * |
| C218 | 0.7430(9) | −0.1529(6) | 0.1836(7) | 3.8(2) * |
| C219 | 0.780(1) | −0.2167(7) | 0.1496(8) | 4.7(3) * |
| C220 | 0.726(1) | −0.2428(8) | 0.0749(9) | 6.1(3) * |
| C221 | 0.641(1) | −0.2098(9) | 0.0349(9) | 7.0(4) * |
| C222 | 0.606(1) | −0.1448(8) | 0.0678(8) | 5.6(3) * |

[a] Anisotropically refined atoms are given in the form of the isotropic equivalent displacement parameter defined as: $(4/3)[a^2B_{1,1} + b^2B_{2,2} + c^2B_{3,3} + ab(\cos\gamma)B_{1,2} + ac(\cos\beta)B_{1,3} + bc(\cos\alpha)B_{2,3}]$.

* Atoms were refined isotropically.

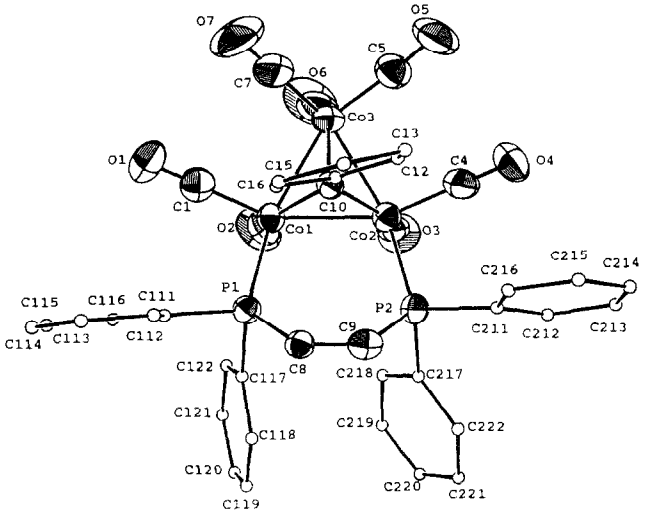


Fig. 2. ORTEP diagram of $PhCCo_3(CO)_7(cis\text{-}Ph_2PCH{=}CHPPh_2)$ with the thermal ellipsoids drawn at the 50% probability level.

data. Selected bond lengths and angles are given in Table 3. The internal polyhedron of **2** consists of a triangular array of cobalt atoms capped by a $\mu_3$-benzylidyne group. The mean value for the Co–Co (2.481 Å) and $\mu_3$-C–Co (1.91 Å) bond lengths are similar to those reported for the parent cluster [25] and related diphosphine-substituted derivatives [1,7,20]. The Co–

TABLE 3. Selected bond distances (Å) and angles (°) in $PhCCo_3(CO)_7(cis\text{-}Ph_2PCH{=}CHPPh_2)$ (**2**)

| | | | |
|---|---|---|---|
| *Bond distances* | | | |
| Co(1)–Co(2) [a] | 2.473(2) | O(2)–C(2) | 1.14(1) |
| Co(1)–Co(3) | 2.483(2) | O(3)–C(3) | 1.14(1) |
| Co(1)–P(1) | 2.206(3) | O(4)–C(4) | 1.16(1) |
| Co(1)–C(1) | 1.75(1) | O(5)–C(5) | 1.16(2) |
| Co(1)–C(2) | 1.79(1) | O(6)–C(6) | 1.15(2) |
| Co(1)–C(10) | 1.88(1) | O(7)–C(7) | 1.17(2) |
| Co(2)–Co(3) | 2.486(2) | C(8)–C(9) | 1.31(1) |
| Co(2)–P(2) | 2.206(3) | Co(2)–C(3) | 1.79(1) |
| Co(2)–C(4) | 1.75(1) | Co(2)–C(10) | 1.90(1) |
| Co(3)–C(5) | 1.75(1) | Co(3)–C(6) | 1.80(1) |
| Co(3)–C(7) | 1.74(1) | Co(3)–C(10) | 1.94(1) |
| O(1)–C(1) | 1.16(1) | P(1)–C(8) | 1.816(9) |
| P(2)–C(9) | 1.81(1) | | |
| *Bond angles* | | | |
| Co(2)–Co(1)–Co(3) | 60.22(6) | C(3)–Co(2)–C(4) | 98.9(6) |
| C(3)–Co(2)–C(10) | 143.0(4) | C(4)–Co(2)–C(10) | 106.7(5) |
| C(1)–Co(1)–C(2) | 99.8(5) | C(1)–Co(1)–C(10) | 107.0(5) |
| C(2)–Co(1)–C(10) | 140.2(5) | C(5)–Co(3)–C(6) | 101.9(6) |
| C(5)–Co(3)–C(7) | 94.0(6) | C(6)–Co(3)–C(7) | 107.2(6) |
| C(6)–Co(3)–C(10) | 141.9(5) | C(7)–Co(3)–C(10) | 96.5(5) |
| Co(1)–P(1)–C(8) | 117.8(4) | Co(2)–P(2)–C(9) | 118.1(3) |
| Co(1)–C(1)–O(1) | 178.(1) | Co(1)–C(2)–O(2) | 175.(1) |
| Co(2)–C(3)–O(3) | 177.(1) | Co(2)–C(4)–O(4) | 178.(1) |
| Co(3)–C(5)–O(5) | 178.(1) | Co(3)–C(6)–O(6) | 178.(1) |
| Co(3)–C(7)–O(7) | 176.(1) | P(1)–C(8)–C(9) | 126.0(8) |
| P(2)–C(9)–C(8) | 128.0(7) | C(10)–C(11)–C(12) | 123(1) |

[a] Numbers in parentheses are estimated standard deviations in the least significant digits.

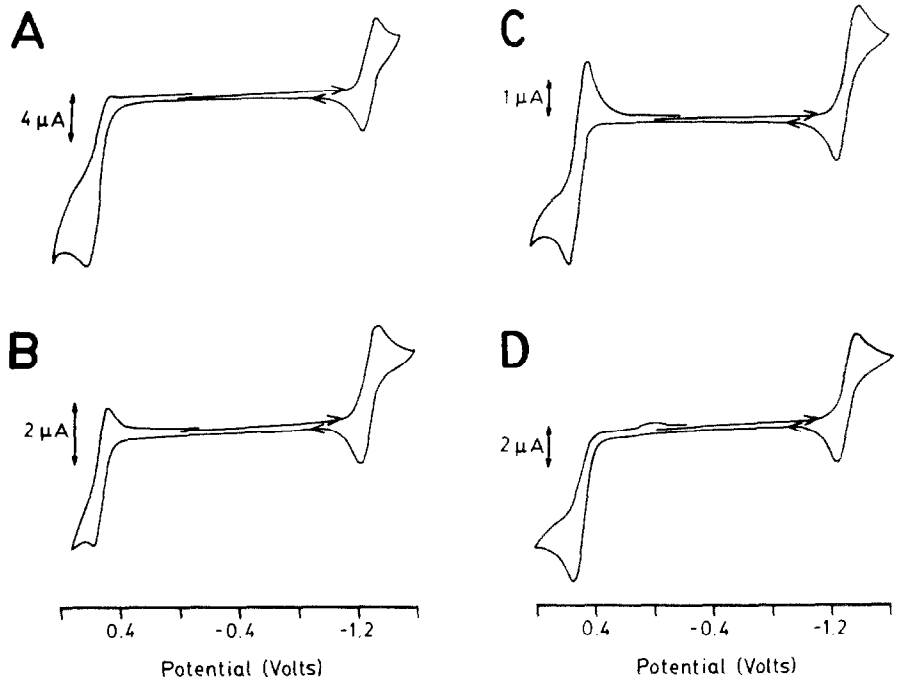


Fig. 3. Cathodic scan cyclic voltammograms of *ca.* $3 \times 10^{-3}$ M $PhCCo_3(CO)_7(cis\text{-}Ph_2PCH{=}CHPPh_2)$ in dichloromethane containing 0.25 M TBAP at $\nu = 0.1$ V/s and (A) 273 K, (B) 228 K, (C) 206 K, and (D) 228 K with 0.1 ml of added MeCN.

CO bond distances range from 1.74(1) to 1.80(1) Å with an average distance of 1.77 Å. The remaining bond lengths and angles are unexceptional and require no additional comments.

### 2.3. Cyclic and rotated disk electrode voltammetric studies

Cyclic voltammetric studies were carried out at a platinum electrode in either $CH_2Cl_2$ or MeCN solution containing 0.25 M tetra-n-butylammonium perchlorate (TBAP) as the supporting electrolyte. Figure 3 shows the cyclic voltammograms (CV) of a recrystallized sample of **2** recorded in $CH_2Cl_2$ solution as a function of temperature and added MeCN. At 273 K, the CV of **2** (Fig. 3(A)) shows a well-defined redox couple at $E_{1/2} = -1.30$ V, which has been assigned to the $0/-1$ redox couple. On the basis of the unity value of the cathodic and anodic peak current ratios ($i_p^c/i_p^a$) at all scan rates examined and the observed linear relationship between the square root of the scan rate ($v$) and the current function ($i_p$), the reduction is judged to be a reversible, diffusion-controlled process [26]. Calibration of the peak current ($i_p^c$) against ferrocene and rotating disk electrode (RDE) voltammetry (*vide infra*) support the one-electron nature of the reduction.

A quasi-reversible oxidation at $E_{1/2} = 0.46$ V is observed and assigned to the $0/+1$ redox couple. The peak current ratio ($i_p^a/i_p^c$) of $\sim 0.2$ is considerably lower than that expected for a reversible, diffusion-controlled, electron-transfer reaction. This behavior indicates that the intermediate radical cation $\mathbf{2}^+$ is extricated rapidly from the vicinity of the electrode, presumably by way of an EC process [26,27]. Increasing the scan rate ($v$) to 5 V/s led to a slight enhancement in reversibility as $i_p^a/i_p^c$ increased to $\sim 0.7$. When **2** was examined out to 1.4 V (not shown), ill-defined waves at $E_p^a = 0.95$ and 1.26 V were also observed. Increasing the scan rate to 10 V/s did not lead to any noticeable reversibility and these additional oxidation waves were not examined further.

The kinetic stability of $\mathbf{2}^+$ is promoted by recording the CV at low temperature. Figures 3(*b*) and (*c*) show the CV of **2** recorded at 228 and 206 K, respectively. The reversibility of the oxidation wave at $E_{1/2} = 0.46$ V improves dramatically as the temperature is lowered, becoming fully reversible at 206 K and readily assignable to the $0/+1$ redox couple [28].

It is interesting that no evidence for the formation of $PhCCo_3(CO)_8(\eta^1\text{-}cis\text{-}Ph_2PCH{=}CHPPh_2)$ or $PhCCo_3(CO)_9$ was observed during these cyclic voltammetric experiments. The dppe-substituted cluster, $PhCCo_3(CO)_7(dppe)$, has been reported to decompose upon reduction to the radical anion, giving the $\eta^1$-dppe cluster and the parent nonacarbonyl cluster [3]. The CV of $PhCCo_3(CO)_7(dppe)$ recorded in $CH_2Cl_2$ solvent at 228 K is identical to that shown in Fig. 3(B). The similarity of the redox potentials between **2** and $PhCCo_3(CO)_7(dppe)$ suggests that the unsaturated carbon backbone in *cis*-$Ph_2PCH{=}CHPPh_2$ does not perturb either the HOMO or LUMO levels in **2** to a measurable extent.

Cyclic voltammograms of **2** recorded in MeCN/0.25 M TBAP (not shown) exhibited a reversible one-electron reduction at $E_{1/2} = -1.35$ V and an irreversible multielectron oxidation wave at $E_p^a = 0.50$ V. The former CV wave is accordingly assigned to the $0/-1$ redox couple while the latter wave is consistent with the generation of $\mathbf{2}^+$ by a one-electron oxidation, followed by solvent interception and decomposition. The overall oxidation is thus best described by a solvent-modulated EC scheme. An analogous process is observed when MeCN is added to **2** in $CH_2Cl_2$/0.25 M TBAP. Figure 3(D) shows the resulting CV after the addition of 0.1 ml of MeCN/0.25 M TBAP to a $CH_2Cl_2$/0.25 M TBAP solution of **2**. The $0/+1$ redox couple is rendered completely irreversible and the presence of an unknown species at $E_p^c = 0.05$ V is noticed. This unknown species is only observable at low temperature. The effect of a polar solvent on the $0/+1$ redox couple in $\mathbf{2}^+$ may be a general phenomenon as the addition of an equivalent amount of THF/0.25 M TBAP afforded a CV identical to Fig. 3d. We are currently investigating the nature of this unknown redox species.

Cluster **2** was also examined at a platinum electrode by rotating disk voltammetry in $CH_2Cl_2$ solvent containing 0.25 M TBAP. The RDE voltammogram shown in Fig. 4 clearly reveals the presence of a well-defined

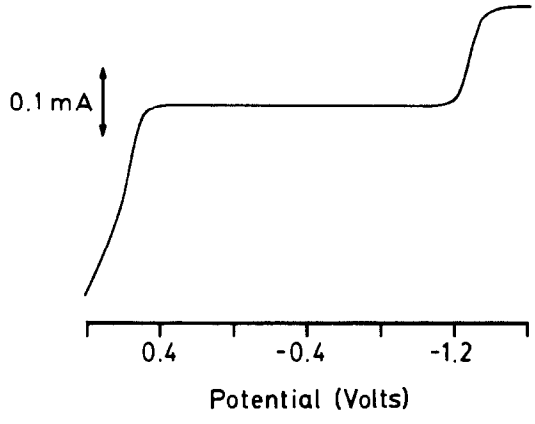


Fig. 4. Anodic scan RPE voltammogram of *ca.* $3\times10^{-3}$ M $PhCCo_3(CO)_7(cis\text{-}Ph_2PCH{=}CHPPh_2)$ in dichloromethane containing 0.25 M TBAP at 273 K and $\nu = 0.05$ V/s.

reduction wave with a half-wave potential ($E_{1/2}$) of $-1.28$ V along with a broad, ill-defined oxidation wave, which results from closely spaced oxidation waves (*vide supra*). The Nernstian nature of the 0/−1 redox couple is verified by a plot of $E$ *vs.* $\log[(i_d - i)/i]$, which reveals a slope close to the theoretically predicted value of 54.2 mV for a reversible, one-electron transfer [26]. Moreover, application of Tomes' criterion for reversibility ($|E_{3/4} - E_{1/4}|$) yields a value of 61 mV, consistent with a reversible, one-electron reduction [29]. No kinetic complications were observed with the 0/−1 redox couple as plot of $i_d$ *vs.* $\omega^{1/2}$ was linear over the electrode rotation rate of 300–1200 rev./min. The diffusion coefficient of **2** has been determined from the slope of the plot of $i_d$ *vs.* $\omega^{1/2}$ using the Levich equation [30]. The experimentally measured value of $3.34 \times 10^{-6}$ cm$^2$/s agrees well with the reported values for other tricobalt clusters of this genre [3] and with the theoretically calculated value of $4.93 \times 10^{-6}$ cm$^2$/s, obtained from the Stokes–Einstein equation, which is shown in eqn. (2) [31*].

$$D = (1 \times 10^7) RT/6\pi rN\eta \qquad (2)$$

## 3. Experimental details

### 3.1. General

Dicobalt octacarbonyl and *cis*-$Ph_2PCH{=}CHPPh_2$ were purchased from Pressure Chemical Co. and used as received. $PhCCo_3(CO)_9$ was prepared according to the procedure reported by Seyferth and co-workers [16]. All reactions were carried out under argon using Schlenk techniques [32]. THF and toluene were distilled from sodium/benzophenone ketyl while $CH_2Cl_2$ and MeCN were distilled from $CaH_2$. All distilled solvents were stored under argon in Schlenk vessels. The tetra-n-butylammonium perchlorate used in the electrochemical studies was purchased from Johnson Matthey Electronics and recrystallized from petroleum ether/ethyl acetate and dried *in vacuo* for 2 days.

Infrared spectra were recorded on a Nicolet 20SXB FT-IR spectrometer in 0.1 mm NaCl cells. The $^{13}C$ and $^{31}P$ NMR spectra were recorded on a Varian 300-VXR spectrometer at 75 and 121 MHz, respectively. The $^{31}P$ chemical shift of cluster **2** was referenced to external 85% $H_3PO_4$, taken to have $\delta = 0$. The positive chemical shift of **2** is to low field of the external standard.

### 3.2. Synthesis of $PhCCo_3(CO)_7$(*cis*-$Ph_2PCH{=}CHPPh_2$)

Since all the procedures utilized similar amounts of $PhCCo_3(CO)_9$ and *cis*-$Ph_2PCH{=}CHPPh_2$ and gave the final product in identical yields, only the thermolysis reaction between $PhCCo_3(CO)_9$ and *cis*-$Ph_2PCH{=}CHPPh_2$ is described in detail.

To a Schlenk tube containing 0.2 g (0.39 mmol) of $PhCCo_3(CO)_9$ and 0.17 g (0.43 mmol) of *cis*-$Ph_2PCH{=}CHPPh_2$ was added 20 ml of toluene *via* syringe. The reaction was heated at ~ 75°C overnight and then allowed to cool to room temperature. TLC examination showed cluster **2** to be the major product. Purification was achieved by using silica gel chromatography with petroleum ether/$CH_2Cl_2$ as the eluant. An analytical sample and crystals suitable for X-ray diffraction analysis were grown from a $CH_2Cl_2$ solution containing **2** that had been layered with heptane. Yield: 0.26 g (78%). IR($CH_2Cl_2$) $\nu$(CO): 2057 s, 2006 vs, 1831 w,b cm$^{-1}$. $^{31}P\{^1H\}$ NMR ($CDCl_3$, 233 K): $\delta$ 36.2. $^{13}C\{^1H\}$ NMR (THF/benzene-$d_6$ (5:1 v/v), 183 K): $\delta$ 211 (2C); 204 (2C); 203 (3C). Anal. Found: C, 54.61; H, 3.20. $C_{40}H_{27}Co_3O_9P_2 \cdot 1/3CH_2Cl_2$ calcd.: C, 54.63%; H, 3.15%.

### 3.3. X-Ray crystallography

A suitable black crystal of dimensions $0.08 \times 0.22 \times 0.43$ mm$^3$ was sealed inside a Lindemann capillary and mounted on the goniometer of an Enraf-Nonius CAD-4 CAD-4 diffractometer employing Mo K$\alpha$ radiation ($\lambda = 0.71073$ Å). The diffractometer was configured with a crystal-to-detector distance of 173 mm and take-off angle of 2.80°. After the crystal was centered in the X-ray beam, an automatic search routine was used to locate up to 25 reflections, which were used to calculate a preliminary cell. After analysis of this initial cell revealed no higher symmetry or centering [33], the cell parameters were refined based on least-squares refinement of 25 reflections with $2\theta > 25°$. Intensity data were collected by using an $\theta$–$2\theta$ scan technique with variable scan width $\Delta\omega = (0.80 + 0.35 \tan\theta)$. Backgrounds were measured by extending the calculated width on either end of the scan by 25%. A fixed vertical detector aperture (4 mm) and a horizontal detector aperture ($3 + \tan\theta$) were used. Reflections with $I/\sigma(I) < 2$ for the prescan were rejected as weak, and those where $I/\sigma(I) > 10$ were accepted after the prescan. Reflections not falling into these two categories were rescanned at speeds ranging from 0.67 to 5.33°/min for up to 120 s in an attempt to increase $I/\sigma(I)$ to 10. Three reflections (6 0 0, 1 −8, 0, 0 0 8) were measured after every 3600 s of exposure time in order to monitor crystal decay (< 1%). Crystal alignment was checked by using the same three reflections every 250 data points, the scattering vectors deviated less than 0.10° from their calculated values throughout data collection. 4786 reflections were collected between $2 < 2\theta < 44°$, with index ranges $+h$, $+k$, $\pm l$, of which 4559 were unique ($R_{merg} = 0.026$).

The intensity ($I$) and standard deviation ($\sigma(I)$) for each reflection were calculated by using eqns. (3) and

(4), respectively, where $C$ is the total number of integrated counts, $B$ is the sum of the left and right backgrounds, $A$ is an attenuation factor (14.3 or 1), and $S$ is the scan rate. The observed structure factors and their standard deviations were calculated by using eqns. (5) and (6), where $L_p$ is a Lorentz polarization correction term, and $p = 0.04$. An absorption correction was applied (DIFABS [34]), but no correction was made for extinction.

$$I = AS(C - 2B) \quad (3)$$

$$\sigma(I) = AS(C + 4B)^{1/2} \quad (4)$$

$$F_o = (I/L_p)^{1/2} \quad (5)$$

$$\sigma(F_o) = \left[\{\sigma(I)^2 + (pI)^2\}\right]^{1/2}/L_p \quad (6)$$

All computations were carried out on a DEC VAXStation 3100/76. Calculations, except where noted, were performed with the MOLEN crystallographic software package [35]. The structure was solved by MULTAN [36] which revealed the positions of the Co and P atoms. All remaining non-hydrogen atoms were located with difference Fourier maps and least-squares refinement. With the exception of the phosphorus phenyl carbons, all non-hydrogen atoms were refined with anisotropic thermal parameters. Hydrogen atoms were generated and allowed to ride on the appropriate carbon [$U(H) = 1.3\ U_{eq}(C)$]. The function minimized during refinement was $\Sigma w(|F_o| - |F_c|)^2$, where $w = 1/(\sigma F)_2$. Final refinement based on 2021 unique reflections with $I > 3\sigma(I)$ converged at $R = 0.0445 = (\Sigma\,|\,|F_o| - |F_c|\,|)/(\Sigma\,|F_o|)$ and $R_w = 0.0488 = [w\Sigma(|F_o| - |F_c|)^2/(w\Sigma(|F_o|^2)]^{1/2}$. The standard deviation of an observation of unit weight = 0.58.

After the final of least squares, the maximum shift of a parameter was less than 0.02 of its estimated standard deviation, and the final difference map showed no feature higher than 0.4 e $Å^{-3}$ (close to C114). Scattering factors were taken from Cromer and Weber [37], and anomalous dispersion effects were included in $F_c$ using the values of Cromer [38]. Plots of $\Sigma w(|F_o| - |F_c|)^2$ *vs.* $|F_o|$, sin $\theta$, or data collection order showed no unusual trends.

### 3.4. Electrochemical measurements

Cyclic and rotating disk electrode voltammetric measurements were conducted with a PAR Model 273 potentiostat/galvanostat, equipped with positive feedback circuitry to compensate for IR drop. The CV cell used was of airtight design and based on a three-electrode configuration, which enabled all cyclic voltammograms to be obtained free from oxygen and water. The CV experiments employed a platinum disk (area = 0.0079 $cm^2$) as the working electrode and a coiled platinum wire as the auxiliary electrode. The RDE voltammograms were recorded in a Vacuum Atmospheres Dribox that was equipped for low-temperature measurements using a PAR Model 616 RDE unit. The working electrode consisted of a commercially available platinum disk electrode (area = 0.126 $cm^2$). All voltammograms utilized a silver wire quasi-reference electrode and all potential data are referenced relative to the formal potential of the $Cp_2/Cp_2Fe^+$ redox couple run under identical conditions, taken to have an $E_{1/2} = 0.306$ V [26].

*Supplementary material available.* Listing of observed and calculated structure factor amplitudes and tables of anisotropic thermal parameters, and idealized hydrogen parameters. Ordering information can be supplied by the authors upon request.

## Acknowledgements

We thank the Robert A. Welch Foundation (B-1202 SGB and B-1039-MGR) and the UNT faculty research program for financial support.

## References and notes

1 G. Balavoine, J. Collin, J.J. Bonnet and G. Lavigne, *J. Organomet. Chem., 280* (1985) 429.
2 J. Collin, C. Jossart and G. Balavoine, *Organometallics, 5* (1986) 203.
3 A.J. Donward, B.H. Robinson and J. Simpson, *Organometallics, 5* (1986) 1122, 1132, 1140.
4 M.I. Bruce, T.W. Hambley, B.K. Nicholson, P.H. Rieger and R.L. Williams, *J. Chem. Soc., Chem. Commun.*, (1982) 442.
5 M.I. Bruce, J.G. Matisons and B.K. Nicholson, *J. Organomet. Chem., 247* (1983) 321.
6 K.A. Sutin, J.W. Kolis, M. Mlekuz, P. Bougeard, B.G. Sayer, M.A. Quilliam, R. Faggian, C.J.L. Lock, M.J. McGlinchey and G. Jaouen, *Organometallics, 6* (1987) 439.
7 W.H. Watson, A. Nagl, S. Hwang and M.G. Richmond, *J. Organomet. Chem., 445* (1993) 163.
8 F. Mao, D.R. Tyler and D. Keszler, *J. Am. Chem. Soc., 111* (1989) 130.
9 F. Mao, C.E. Philbin, T.J.R. Weakley and D.R. Tyler, *Organometallics, 9* (1990) 1510.
10 F. Mao, S.K. Sur and D.R. Tyler, *Organometallics, 10*, (1991) 419.
11 F. Mao, D.R. Tyler, A.L. Rieger and P.H. Rieger, *J. Chem. Soc. Faraday Trans., 87* (1991) 3113.
12 D.R. Tyler, *Acc. Chem. Res., 24* (1991) 325.
13 D. Fenske and H.J. Becher, *Chem. Ber., 107* (1974) 117.
14 D. Fenske, *Chem. Ber.*, 112 (1979) 363.
15 K. Yang, J.M. Smith, S.G. Bott and M.G. Richmond, unpublished results.
16 M.O. Nestle, J.E. Hallgren and D. Seyferth, *Inorg. Synth., 20* (1980) 226.
17 (a). M.O. Albers and N.J. Coville, *Coord. Chem. Rev., 53* (1984) 227; (b) T.-Y. Luh, *Coord. Chem. Rev., 60* (1984) 255.

18 (a) M.I. Bruce, *Coord. Chem. Rev.*, *76* (1987) 1; (b) M.G. Richmond and J.K. Kochi, *Organometallics*, *6* (1987) 254.
19 P.E. Garrou, *Chem. Rev.*, *81* (1981) 229 and refs. therein.
20 M.-J. Don, M.G. Richmond, W.H. Watson, M. Krawiec and R.P. Kashyap, *J. Organomet. Chem.*, *418* (1991) 231.
21 S. Aime, L. Milone, R. Rossetti, and P.L. Stanghellini, *Inorg. Chim. Acta*, *25* (1977) 103.
22 (a) M.J. Don and M.G. Richmond, *Inorg. Chem.*, *30* (1991) 1703; (b) P. Yuan, M.G. Richmond and M. Schwartz, *Inorg. Chem.*, *30* (1991) 679; (c) P. Yuan, M.-J. Don, M.G. Richmond and M. Schwartz, *Inorg. Chem.*, *30* (1991) 3704; (d) R.A. Gates, M.F. D'Agostino, K.A. Sutin, M.J. McGlinchey, T.S. Janik and M.R. Churchill, *Organometallics*, *9* (1990) 20.
23 The possibility of a chelate/bridge equilibrium reaction involving $PhCCo_3(CO)_7(cis\text{-}Ph_2PCH{=}CHPPh_2)$ has been raised by a reviewer in connection with spectrum in fig. 1(*c*). Since the amount of the chelating isomer remains unchanged relative to the bridging isomer in a variety of solvents, it has been assumed that these isomers do not interconvert with each other under the conditions of this study.
24 (a) H. Shanan-Atidi and K.H. Bar-Eli, *J. Phys. Chem.*, *74* (1970) 961; (b) J. Sandström, *Dynamic NMR Spectroscopy*, Academic Press, New York, 1982.
25 (a) S.B. Colbran, B.H. Robinson and J. Simpson, *Acta Crystallogr. Sect. C.*, *42* (1986) 972; (b) M. Ahlgrén, T.T. Pakkanen and I. Tahvanainen, *J. Organomet. Chem.*, *323* (1987) 91.
26 A.J. Bard and L.F. Faulkner, *Electrochemical Methods*, Wiley, New York, 1980.
27 P.T. Kissinger and W.R. Heineman, *Laboratory Techniques in Electroanalytical Chemistry*, Marcel Dekker, New York, 1984.
28 M.G. Richmond and J.K. Kochi, *Inorg. Chem.*, *25* (1986) 656.
29 J. Tomeš, *Coll. Czech. Chem. Commun.*, *9* (1937) 12, 81, 150.
30 V.G. Levich, *Physicochemical Hydrodynamics*, Prentice Hall; Englewood, Cliffs, NJ, 1962.
31 (a) A.W. Adamson, *Understanding Physical Chemistry*, W.A. Benjamin, New York, 1969, (b) where $R$ is the gas constant $T$ is the absolute temperature, $r$ is the molecular radius, which was obtained from the observed molecular volume of the crystal structure, $N$ is Avogradro's number and $\eta$ is the solvent viscosity.
32 D.F. Shriver, *The Manipulation of Air-Sensitive Compounds*, McGraw-Hill, New York, 1969.
33 *CAD4 Operations Manual*, Enraf-Nonius; Delft, The Netherlands, 1989.
34 N. Walker and D. Stuart, *Acta Crystallogr., Sect. A*, *39* (1983) 159.
35 MolEN, *An Interactive Structure Solution Program*, Enraf-Nonius, Delft, The Netherlands, 1990.
36 P. Main, S.J. Fiske, S.E. Hull, L. Lessinger, G. Germain, J.P. DeClerq and M.M. Woolfson, MULTAN 80: A System of Computer Programs for the Automatic Solution of Crystal Structures from X-Ray Diffraction Data, University of York, UK, 1980.
37 D.T. Cromer and J.T. Weber, *International Tables for X-Ray Crystallography*, Vol. IV, Kynoch Press, Birmingham, UK, 1974, Table 2.
38 D.T. Cromer, *International Tables for X-Ray Crystallography*, Vol. IV, Kynoch Press, Birmingham, UK, 1974, Table 2.3.1.